



Vision based autonomous docking for work class ROVs

Petar Trsllic ^{*}, Matija Rossi, Luke Robinson, Cathal W. O'Donnell, Anthony Weir, Joseph Coleman, James Riordan, Edin Omerdic, Gerard Dooly, Daniel Toal

Centre for Robotics and Intelligent Systems (CRIS), University of Limerick, Limerick, Ireland

ARTICLE INFO

Keywords:
Resident ROV
Autonomous docking
Computer vision

ABSTRACT

This paper presents autonomous docking of an industry standard work-class ROV to both static and dynamic docking station (Tether Management System — TMS) using visual based pose estimation techniques. This is the first time autonomous docking to a dynamic docking station has been presented. Furthermore, the presented system does not require a specially designed docking station but uses a conventional cage type TMS. The paper presents and discusses real-world environmental tests successfully completed during January 2019 in the North Atlantic Ocean. To validate the performance of the system, a commercial state of the art underwater navigation system has been used. The results demonstrate a significant advancement in resident ROV automation and capabilities, and represents a system which can be retrofitted to the current ROV fleet.

1. Introduction and background

There is constant growth in the world's energy consumption and an ever-increasing focus on energy security and diversification, with an emphasis on having energy production within home territorial regions. With expansion comes increased demand for all fuels and we have seen all variants except coal and hydroelectricity grow at above-average rates (Dudley, 2018). In recent years the trend in offshore power generation, both in oil & gas (O&G) and marine renewable energy (MRE), is to move production platforms further offshore where significant energy potential exists (W. Europe, 2017). This trend comes from a number of contributing factors including: need for increased energy farm footprint, technological advancements in ROV/AUV industry and significant savings in deep-water capital expenditure (CAPEX) and operational expenditure (OPEX) costs compared to 2014 levels (Intelligence, 2019). However and although higher energy potential and cost savings have resulted in deep-water sites becoming commercially viable, the costs associated with operations, maintenance, and repair are inevitably increasing with the move into deeper offshore regions. In downtime/failures, due to the remoteness of the production platform and associated transit times, weather windows for Inspection Maintenance and Repair (IMR) operations are significantly reduced. This represents a substantial issue in reducing and maintaining projected OPEX costs. This may not be overcome simply through predictive maintenance due to the growth in infrastructure planned within the future offshore blue economy. One of the primary OPEX costs including ROV deployment, is support vessel day rates. The day rate of an offshore maintenance vessel with a crew and equipped with ROV typically

reaches at 100.000\$ or more (Statoil, 2017; Christ and Sr, 2013). While production platform downtime can cause considerable costs in the O&G industry, geographic spread of infrastructure assets creates additional concerns within the MRE sector, which is currently undergoing huge expansion. Floating offshore MRE farms consist of seabed infrastructure, anchoring systems, flexible cable risers, floating platforms, towers, and distributed buoys/sensors that can be spread over an area of 100 km² or more. IMR tasks on a huge area demand more vessels, thus introducing higher OPEX. Furthermore, weather conditions onsite are more adverse further offshore, and considering that MRE sites are by their nature located in strong wind/current/tide areas, there can be narrow windows for IMR operations. The primary restriction in terms of ROV operations and associated operational weather windows, is in the launch and recovery of the vehicle, and the most demanding time for the pilot is within the first 15 m of water depth. These restrictions are recognised within the industry, particularly within the offshore wind sector, and as a solution to the problems resident, permanently deployed underwater vehicles are emerging as a potential solution to overcome these problems, expand operation weather windows and reduce OPEX costs. Using a permanently deployed vehicle, real-time, weather independent, onsite remote piloting is possible. This opens the path to year-round operations without the need for expensive vessels onsite and with reduced personnel transfers (OSJ, 2018).

ROVs have been the workhorse of the oil & gas industry since their introduction in the early 1970s, however the resident ROV concept is only recent, being born out of unprecedeted cost saving demand

* Corresponding author.

E-mail address: petar.trsllic@ul.ie (P. Trsllic).

for O&G and global expansion of the offshore wind sector. There are various research and development projects globally investigating this concept, some with significant collaboration and investment from both the oil & gas and the MRE industry sector. Two major investments in work-class resident ROV systems are led by Oceaneering and IKM. Oceaneering developed the resident ROV solution E-ROV (Equinor, 2019) for Equinor (formerly Statoil). The E-ROV system consists of a work class ROV and tether management system (TMS) stationed on the seabed, with a fully integrated communication system buoy on the surface. The power is supplied through submerged battery pack which can be scaled up or down, depending on operational requirements (Oceaneering, 2019; OSJ, 2018). This system represents an intervention ROV system, which is mobile and can be redeployed relatively easily. Based on E-ROV, Oceaneering also released details of a new vehicle called Freedom, currently under development. Freedom represents a concept move towards a system in a hybrid ROV/AUV format. While in AUV mode, this system would be primarily mobile through the limited onboard power while moving between multiple sites spread around operational field. After Freedom approaches the site, it reconnects to a subsea charging and communication station and allows for a real time ROV piloting. The other major industrial research project in resident systems is ongoing between Equinor and IKM. Through this collaboration IKM developed a large resident system for heavy intervention in an O&G field called R-ROV. It consists of a Launch and Recovery System (LARS) and power supply system deployed on a floating platform (e.g. O&G platform) with a TMS and docking station deployed to the seabed (UT2, 2018; IKM Subsea, 2018). The communication channel to the shore-based ROV operating centre is provided through satellite uplink/downlink (Robinson et al., 2018), 4G mobile network or in some cases fibre optic cable piggybacked on existing pipeline infrastructure. There are several examples of resident hybrid ROV/AUV projects, based around vehicle platforms which can transition between ROV and AUV mode, which are in different stages of development and technology readiness level (TRL) phases. The primary advantage of this hybrid concept is that it can unplug itself, operate in AUV mode and autonomously move location to a second subsea resident station, covering relatively long distances with the onboard battery pack. Once a resident station is reached the ROV reconnects. Saipem is working on the Hydrone family of resident ROVs (UT2, 2018), while Eelume is focused on a snake-like ROV for navigating through tight places (Liljeback and Mills, 2017). Another example is the ROV Clean sea project, developed by Eni and based on the use of the Saab Sabertooth commercial ROV/AUV (Grasso et al., 2016) with the objective of environmental monitoring in offshore O&G fields (Buffagni et al., 2014). In general, there has been a significant uptake of commercial interest in resident ROV systems, with various research targeting different problems within the field reported (Omerdic et al., 2014; Ferri and Djapic, 2013). This has resulted in significant investment into development of early phase TRL projects. However, many of the examples in the literature fail to address some of the fundamental barriers to the rollout of this technology into commercial sectors.

Fundamentally resident ROVs operating from shore demand a high bandwidth, low latency communication link which is in most cases unavailable. Therefore, to achieve the level of agility needed for resident ROVs in subsea domains and within time-critical tasks, these communication issues need to be addressed. High levels of automation, through onboard sensor technologies, machine learning, computer vision, and advanced control and navigation approaches can provide an alternate to the high-bandwidth communication link requirements for remote on shore piloting solution (Dooly et al., 2016). One of the critical tasks in resident ROV operations is the docking of the system back into the docking station (DS) at the end of a mission. This is a particularly crucial part of all ROV operations and likely represents the primary task which will dictate the full system operating window. Research in the literature on the automation of subsea vehicle docking procedures has been focused on AUV platforms, allowing for recharging

and data exchange without recovering to surface. Estimation of the relative position between the vehicle and the docking station includes approaches such as an electromagnetic homing systems (Feezor et al., 2001) and an optical terminal guidance systems (Cowen et al., 1997). Autonomous docking based on use of an ultra-short baseline (USBL) system was demonstrated in Allen et al. (2006) while visual based pose estimation has also been recorded (Krupinski et al., 2008; Gracias et al., 2015; Bosch et al., 2016; Zhong et al., 2019). Similar problems are faced in space industry for spacecraft docking (Fehse, 2003) targeted with different visual pose estimation methods (Mokuno and Kawano, 2011; Yu et al., 2014; Liu et al., 2019b).

1.1. Scope of work

This paper presents autonomous docking of an industry standard work-class ROV to both (a) static and (b) suspended TMS using a visual based pose estimation approach. Evaluation of the system has been demonstrated through completion of offshore trials in the North Atlantic Ocean in January 2019. Although docking of AUVs with pose estimation based on image acquisition already exists (Park et al., 2009; Li et al., 2015; Vallicrosa et al., 2016), research in the literature mainly focuses on development and docking to a static docking station, usually attached to the seabed. While systems facing with the docking of vehicle to moving docking stations are reported (Fornai et al., 2013; Conte et al., 2016; Liu et al., 2019a), to our knowledge, this is the first autonomous docking of an ROV system to a suspended TMS within the water column. Furthermore, the approach taken does not require specific narrowing entry/funnel shape designs on the docking station. This approach has the dual benefit of minimising mechanical complexity and footprint needed and enabling the possibility to retrofit to the existing ROV fleet. In comparison to the funnel-shaped AUV receptacle (Allen et al., 2006; Park et al., 2009; Vallicrosa et al., 2016), a significant difference lies in the vehicle to DS entrance size ratio. The entrance nozzle of AUV docking stations is 4 to 5 vehicle diameters (Allen et al., 2006; Palomeras et al., 2018), whereas entrance of the TMS used as a docking station in this paper is approximately 1.3 times the vehicle size. Accurate position sensing and advanced ROV control described herein allows for this docking manoeuvre.

2. ROV docking

Docking of a ROV system is one of the fundamental tasks which dictates operation weather windows. It takes a pilot's full concentration and skill, with decisions being undertaken in a fraction of a second while controlling the ROV. There are two major types of TMS systems. A top hat TMS and a cage-type TMS (Christ and Sr, 2013). A cage-type TMS was used during the trials reported in this paper.

2.1. Manual ROV docking

Manual docking into a cage-type TMS starts with the ROV stern facing the entrance of the TMS as illustrated in Fig. 1. During the docking procedure a pilot first matches heading, depth, and lateral alignment of the vehicle relative to the TMS. The vehicle approaches the entrance of the TMS slowly. While still in front of the TMS the pilot estimates the amount of heaving motion. At this moment there is a low amount of tension present in the tether connecting the TMS and ROV. Since work class ROVs are generally not agile enough to match TMS heaving motion due to large inertia, the pilot waits for the right moment when the entrance of the TMS and the ROV are aligned. At the appropriate moment, a light forward thrust is applied to the ROV while a 'tether in' command is given. The light ROV forward thrust keeps the tether under tension as the ROV is docked. With taut tether the ROV moves backwards as we start tethering in due to the tether tension. It may seem counterintuitive, but the forward thrust is applied

Table 1
Technical specification of the system.

	Description	Dimensions L × W × H [m]	Weight [t]
Control Cabin	Reinforced container used as ROV control centre	6 × 2.4 × 2.4	6.5
LARS	A - frame type, 2200 m steel enforced umbilical, ϕ 25.4 mm	5.5 × 2.8 × 3.2	12
TMS	Cage-type, 400 m soft tether, ϕ 21 mm	2.9 × 1.8 × 2.5	2.1
ROV	Middle size ROV capable of inspection, maintenance and repair tasks	2.1 × 1.3 × 1.25	1.1
Ship	Research Vessel	Length — 66 m Displacement — 2425 t	

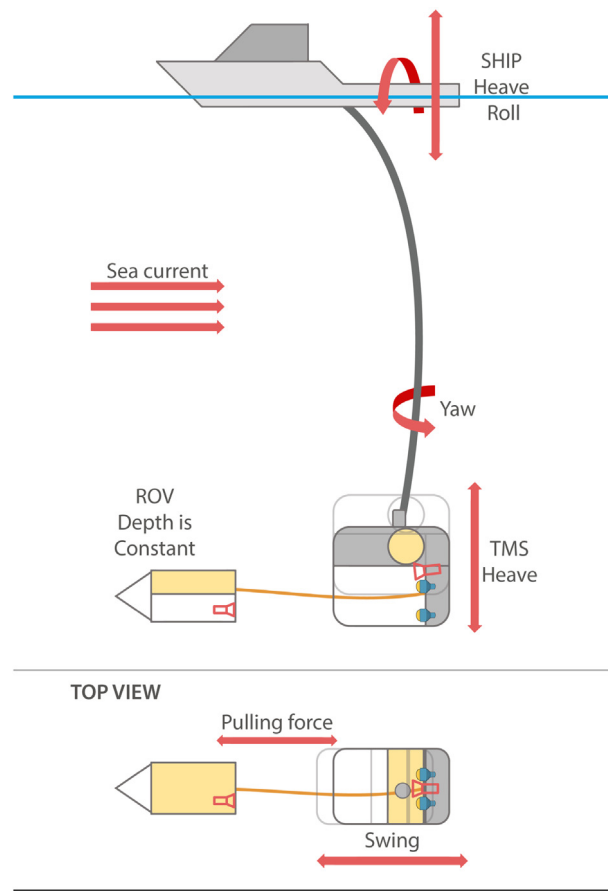


Fig. 1. Major disturbances acting on TMS.

to maintain a constant tension on the tether which allows for best spooling performance and lowers the risk of tangling the tether.

Three major disturbances potentially act upon a TMS during such a docking procedure:

- The sea current/wave motion
- The tether pulling force between the ROV and the TMS
- Rolling and heaving motion of the surface ship, translated to the TMS through the Launch and Recovery System (LARS) as a heaving motion

The sea current is a disturbance, usually in a horizontal direction, that acts upon the tether, TMS and the ROV. Since the TMS acts as a clump weight as well, it absorbs the cross-section drag. Thus the ROV is relieved of the tether drag from the surface to the working depth. Therefore the ROV needs to compensate only for vehicle drag and tether drag introduced on soft tether between TMS and the vehicle. However, since the TMS is suspended in one point, the sea current generally rotates the TMS around the yaw axis to an orientation that creates the least amount of drag. The TMS stays in such yaw orientation as long as tension in the tether connecting the ROV and the TMS, do not cause a rotating moment. The tension in tether can produce a swinging

pendulum motion of the TMS in the direction of the ROV. There are two sources of TMS heave motion. Since the TMS is suspended from a ship, the amount of heave introduced to a ship through waves, directly translates to the TMS. As shown in Fig. 2, the TMS was deployed from the starboard side of the ship. Therefore a roll motion of the ship generates a TMS heave motion through the LARS acting as a lever arm. A TMS heave motion can be reduced if a heave compensating winch is employed, which was not available during the trials. One of the main objectives of the LARS is to move the ROV and TMS through the splash zone safely to the working depth. Close to the surface, the ROV could easily be overpowered by the waves. This would lead to possible contact between the ROV, TMS, and the ship hull. To avoid direct impact of waves on the TMS and the ROV, which could possibly lead to severe damage, the docking is generally performed below the splash zone at depths of 20 m or more.

In summary, the relative motion of the ROV and TMS may have a combination of heave, yaw, and pendulum swing motion. It is generally not possible to compensate for all the motion, thus docking regularly involves a rough contact bump between the ROV and TMS, which are designed for such.

3. Hardware

Fig. 2 shows the experimental setup used for autonomous docking. The industry standard equipment was used with upgraded, in house developed control systems. The Centre for Robotics and Intelligent Systems (CRIS), University of Limerick ROV system consists of a control cabin, launch and recovery system (LARS), tether management system (TMS), and the remotely operated vehicle ROV Étaín itself. Technical specifications of the system components are given in Table 1. The Research Vessel (RV) Celtic Explorer ([M. Institute, 2019](#)) was used throughout the offshore trials.

The ROV is controlled from a control cabin used as the control centre aboard the research vessel. Power is supplied from the ship, while the connection between the cabin and the TMS and ROV is established through 2.2 km of steel reinforced umbilical with embedded fibre optic cable. The LARS is a conventional A-frame type, hydraulically operated unit.

3.1. ROV and TMS

ROV Étaín is a Sub Atlantic fully electric Comanche ROV with onboard hydraulic power used for manipulators and tooling. The ROV is equipped with an inertial navigation system coupled with a Doppler Velocity Log (DVL), and an additional Ultra Short Baseline (USBL) system to eliminate navigation drift solution. The vehicle is equipped with four horizontal and three vertical thrusters and can achieve a maximum speed of 2.5 knots. The ROV buoyancy was trimmed to be slightly positive, which in case of severe damage would bring the ROV to the surface. The ROV weights approximately 1650 kg in the air, and it is docked to a cage type, side entry TMS, which is used as a docking station.

Fig. 3 shows an overview of the TMS and ROV system with the overall dimensions relevant for docking. The TMS is a conventional Comanche ROV TMS and is not designed to operate as an auto-docking station. The ROV fits tightly within the TMS. The red shaded area in the figure shows the funnel-shaped TMS entrance which helps to physically

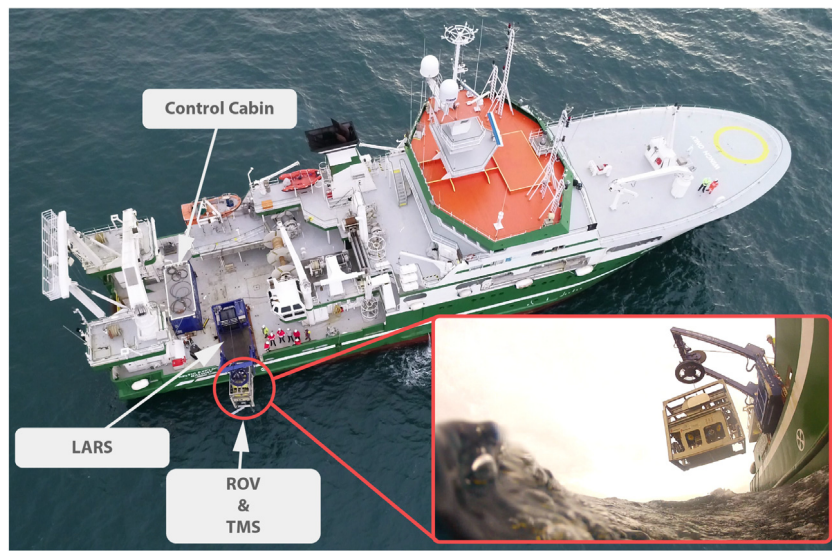


Fig. 2. Experimental setup overview.

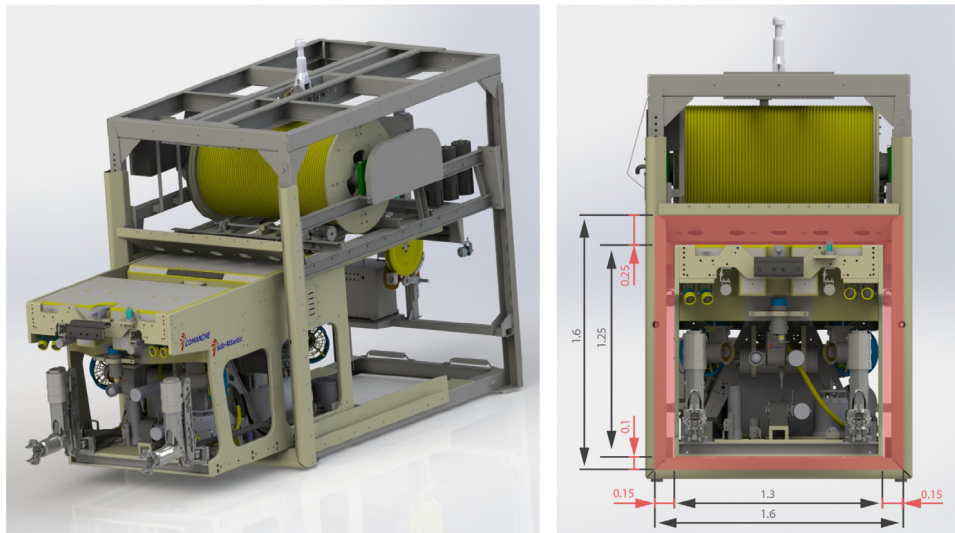


Fig. 3. The TMS and ROV system overview with overall dimensions [m]. The funnel shaped entrance allows small ROV-TMS misalignment (red shaded area). (For interpretation of the references to colour in this figure legend, the reader is referred to the web version of this article.)

guide the vehicle. The entrance allows only for a small misalignment during the docking procedure, thus makes the auto-docking task more challenging.

To accommodate one of the planned tests, that of docking to a static docking station, the TMS has been slightly modified. Fig. 4 shows four legs mounted on each corner of the TMS to create clearance of the TMS from the seabed and thus allow static docking manoeuvres. The legs are 0.8 m long, which is enough to safely operate the ROV without disturbing the stability of the TMS.

3.2. Navigational lights for docking

To complete testing of algorithms for lights recognition and pose estimation prior to any mobilisation for offshore missions, a simple rig to test the developed software was built. A plywood board was used as the rig body with 100×100 mm inscribed squares, which form a raster for the different light patterns and configurations that were tested. An optimal light beacons arrangement has been achieved taking into account the camera Field of View (FOV), robustness to light

saturation, and possible camera mounting positions on the ROV. Conventional, off the shelf, LED light bulbs were used. The light beacons have been arranged asymmetrically to uniquely define the orientation of the light marker. The vision system does not necessarily require the overall marker to be asymmetrical. In that case the orientation of the vehicle has to be assumed or measured with additional sensor. For example, if rectangular marker is used, the vehicle orientation is not uniquely defined, and there are two possible solutions. The ROV is either oriented normally or it is rotated 180° around roll axis. To determine the ROV orientation a measurement from the onboard INS system can be used. Otherwise, the orientation can be assumed based on the mechanical properties and the design of the ROV. Since the ROV centre of buoyancy is above the centre of gravity, positive longitudinal and lateral stability is achieved. Therefore, the vehicle is stable on the pitch and roll axis, and the orientation of the vehicle can be assumed with certain probability, yielding unique solution. Fig. 5 shows the test rig with light beacons attached to it forming different asymmetrical patterns.

The analysis of the propagation of the light through seawater is a well established area of research (Duntley, 1963; Haltrin, 1999).



Fig. 4. The ROV within the TMS with four legs retrofitted for the static docking experiment prior to launch.

The research shows that the red spectre of light is highly attenuated in deep ocean water while the blue light attenuates at much less degree. Low attenuation property can be shifted towards the green light in coastal areas with yellow solutes which result from the plant and animal materials decomposition. Therefore, the property of blue light penetration in sea water is often used in subsea wireless optical communications field (Pontbriand et al., 2008; Cai et al., 2016), for AUV visual based docking (Cowen et al., 1997; Liu et al., 2018) and underwater object detection and tracking (Lee et al., 2012). However, the scope of the paper is to use existing industry-standard technology, thus the lights used for the visual pose estimation are conventional, off the shelf Bowtech LED-K-3200-DC underwater lights, rated to 3000 m. This type of lights is typically used on the TMS systems, ROVs, trenchers and other subsea structures for better visibility in a dark or



Fig. 6. IDS uEye camera used for the experiment.

turbid environment. Therefore, the existing TMS lights were remounted to form an asymmetrical pattern, which is to be recognised by the camera. The lights are mounted at the back of the TMS using aluminium profiles.

3.3. Camera

The machine vision camera used for testing and trials is a Power over Ethernet (PoE), IDS uEye (UI527xCP-C) GigE with Sony 1/1.8" CMOS (IMX265) sensor. The maximum resolution of the camera is 2056 × 1542 pixels. Horizontal and vertical subsampling is used to reduce network overload and to achieve a higher sample rate. The camera is enclosed in a subsea housing rated to 2000 m, as shown in Fig. 6.

A Lensagon BM4518S lens with fixed focus is used. The camera housing has a flat port and the lens is not wide angle, thus the FOV is reduced significantly due to light refraction in water. To achieve the widest possible FOV the authors suggest using dome ports and wide-angle lenses.

The acquired image is sent via the ROV network to a dedicated topside PC where image processing is done. The physical network layer consists of an optical fibre enclosed in 2.2 km steel reinforced umbilical connecting the ROV cabin with the TMS, and 400 m of soft tether connecting the TMS and the ROV. The Gigabit network uses the TCP/IP protocol. Due to the ROV design, which requires reversing into the TMS while docking, the camera is mounted at the stern of the ROV and faces backwards.

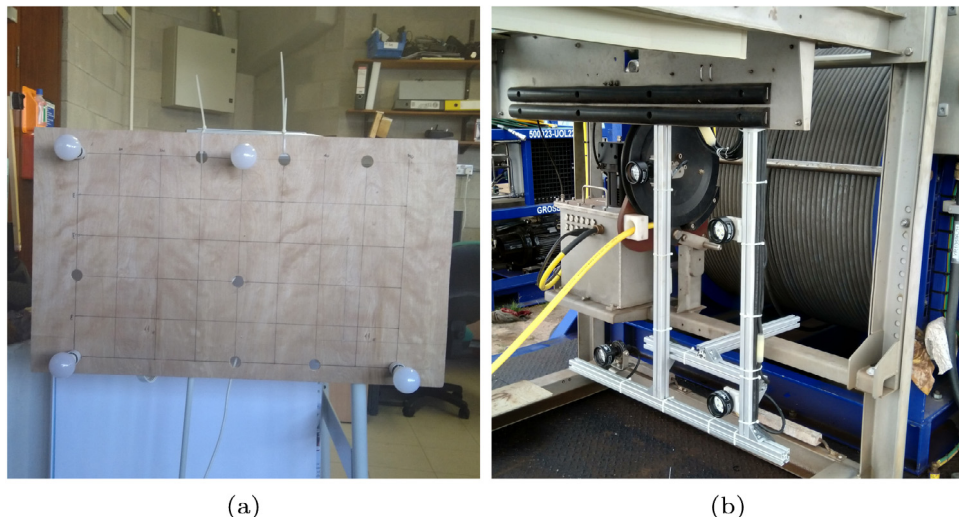


Fig. 5. Navigational lights (a) test rig; (b) on the TMS.

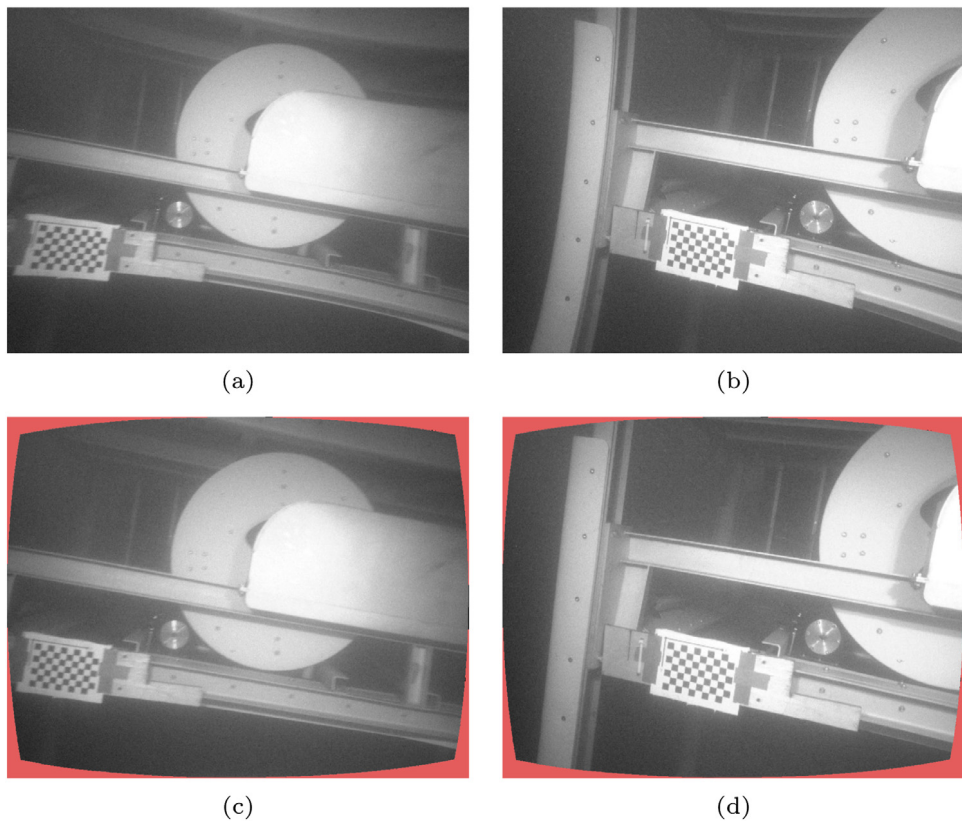


Fig. 7. Comparison between images before and after the calibration process. (a)(b) original images with distortion; (c)(d) undistorted images.

4. Autonomous docking

This section describes the auto-docking methods developed for the experiment. Image acquisition and processing was implemented on the surface using a dedicated computer. The ROV control is part of the OceanRINGS+ (Omerdic et al., 2013; Sivčev et al., 2018; Rossi et al., 2018) software developed within the research group. The image processing PC and the ROV control PC communicate through the network using the UDP protocol.

4.1. Camera calibration

The camera must be calibrated before the beginning of the experiment, and although methods to pre-calibrate in air exist (Luczyński et al., 2017) the best practice is to acquire calibration parameters on site. The calibration panel used for the calibration process is a 7×10 chessboard pattern printed on an A4 sized PVC board. The panel was mounted on the port side of the TMS and deployed in water. The ROV was manually manoeuvred around the TMS while images of the panel were acquired from different angles.

The images were processed, and intrinsic camera parameters derived. The calibration algorithm assumes a pinhole camera model (Hartley and Zisserman, 2004). Fig. 7 shows images with a chessboard pattern attached to the TMS. Approximately 50 images were taken from different angle and distance combinations. Acquired lens distortion and intrinsic parameters of the camera are used to correct image distortion, thus providing better pose estimation. Since the emphasis of the paper is on ROV docking procedures in the remainder of this paper term docking station (DS) is used for TMS.

4.2. Image acquisition and pose estimation

Image acquisition and processing software has been implemented in MATLAB on a dedicated computer located in the ROV control cabin.

An interface between the camera used during the trials and MATLAB does not exist, thus a MEX file based on [uEye Camera Interface in Matlab \(2016\)](#) was created in order to use the C++ SDK provided by the camera manufacturer. The term MEX stands for 'MATLAB executable'.

The relative position between the ROV and the docking station (DS) is estimated using a single camera and a light marker of a known size. The light marker consists of four light beacons mounted on the aluminium frame. The frame with the marker is mounted on the DS as shown previously in Fig. 5. To avoid ambiguity, the light beacons were mounted asymmetrically, thus creating a unique light marker. A similar approach was used in Palomeras et al. (2018) where active light beacons with known blinking patterns were used in order to avoid the same problem.

The image processing steps are shown in Fig. 8. The process starts with image acquisition (a). Distortion is then removed based on known camera intrinsic parameters obtained through the camera calibration (b). To avoid problems related to light scatter, as mentioned in Park et al. (2009), camera exposure is set to a value where only strong sources of light (relative to surroundings) can be detected. A Gaussian filter is used to blur the image in the next step (c). Image blur is used as a low pass filter which averages out the pixel intensities. Although by adding blur more detail is being removed, the position of the brightest objects in the image (light beacons) is not changed, thus the precision is not reduced while robustness is achieved. Additionally salt and pepper noise could occur during the image acquisition and transmission, and affect the binarization of the image in the last step. In that case a non-linear filter from the group of Median filters should be used (Chan et al., 2005; Esakkirajan et al., 2011). In the last step, the image is thresholded and the centres of the four detected disc-shaped objects are calculated (d). The image threshold function returns a binary image from a greyscale image by replacing all values that are above a globally determined threshold with the value 1, while setting all other values to 0. If the image is not blurred, small reflections from metal objects or the ROV tether can be detected, as shown in 8(e).

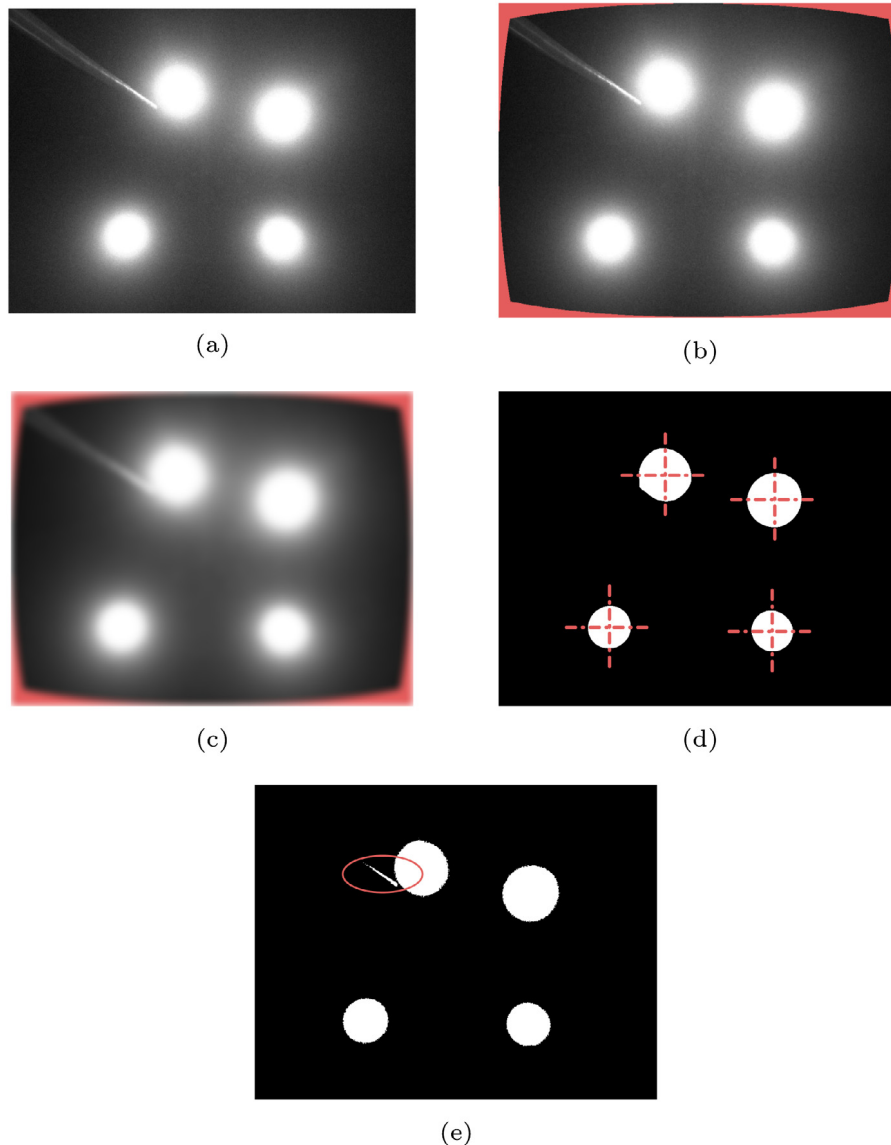


Fig. 8. Image processing stages. (a) captured frame; (b) image distortion removed; (c) Gaussian filter applied to average out pixel intensities; (d) blurred binarized image with calculated centres of the light markers; (e) non blurred binarized image, reflection from tether present (circled).

Ideally, the binary image returns four perfectly disc shaped objects with calculated centres of objects matching the centres of the real light beacons. Based on the known distance between the centres of the four light beacons and known camera parameters, a transformation matrix between two planes can be computed, providing information about all six degrees of freedom.

The coordinate systems used in this section are shown in Fig. 9. The docking station *DS* reference frame is considered the fixed world frame and it is defined by four light beacons, with the *XY*-plane being coplanar with the plane passing through the centres of the light beacons. The origin of *DS* frame can be arbitrary point in that plane. Once the origin of the frame is chosen the relative distance between the light beacons and the origin is measured as shown in Fig. 10. The measured distances present a world coordinates of light beacons B^{DS} . In practice the origin of *DS* frame is chosen to align with the camera frame when ROV is docked and latched.

Given the world coordinates of light beacons B^{DS} , their corresponding image coordinates I_B , and intrinsic camera parameters K , the extrinsic camera parameters are calculated as:

$$[R_{\text{CAM}}^{\text{DS}}, t_{\text{CAM}}^{\text{DS}}] = E(B^{\text{DS}}, I_B, K), \quad (1)$$

where B^{DS} is an $M \times 3$ matrix with at least $M = 4$ coplanar points, I_B is a corresponding $M \times 3$ matrix, $R_{\text{CAM}}^{\text{DS}}$ is a 3-D rotation matrix, and $t_{\text{CAM}}^{\text{DS}}$ is a 3-D translation vector.

The transformation of points from the docking station frame to the camera frame therefore is:

$$p_N^{\text{CAM}} = p_N^{\text{DS}} R_{\text{CAM}}^{\text{DS}} + t_{\text{CAM}}^{\text{DS}}, \quad (2)$$

where p_N^{CAM} is the position vector of point N in the camera frame with coordinates $[x_N^{\text{CAM}}, y_N^{\text{CAM}}, z_N^{\text{CAM}}]$ and p_N^{DS} is the position vector of point N in the *DS* frame.

The vehicle control system is designed to operate in the *ROV* coordinate frame. The *ROV* frame is defined as the intersection of lines connecting the centres of diagonally placed thrusters. The transformation of any point N from camera frame to *ROV* frame is defined as:

$$p_N^{\text{DS}} = p_N^{\text{CAM}} R_{\text{ROV}}^{\text{CAM}} + t_{\text{ROV}}^{\text{CAM}}. \quad (3)$$

The position error between the docking point *DP* and the origin of the *ROV* frame is used to calculate setpoints for position and speed controllers. When *DP* overlaps with the origin of the *ROV* frame, the vehicle is considered docked.

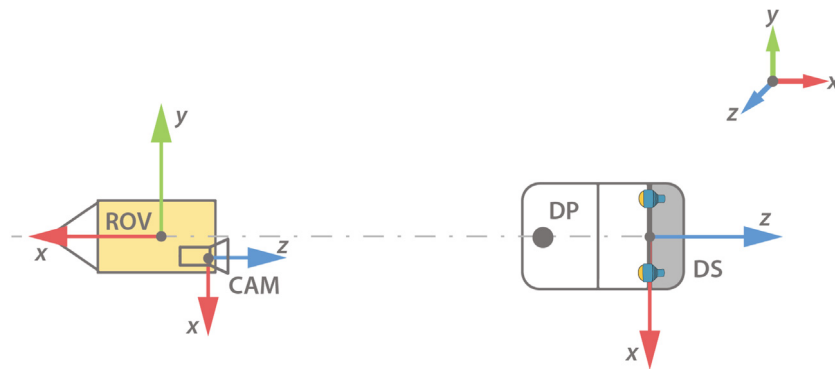


Fig. 9. Coordinate systems — top view.

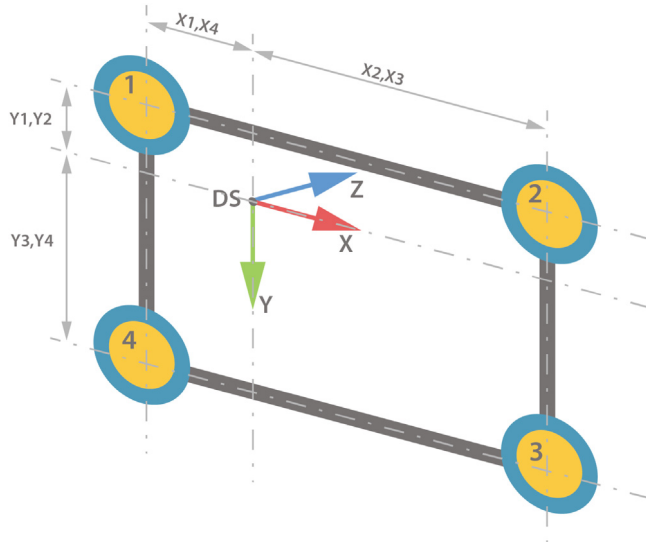


Fig. 10. Origin of *DS* reference frame is coplanar with the plane passing through the centres of the light beacons. The relative distance between centres of light beacons and the origin of the frame present the world coordinates.

Therefore, given the docking point *DP* in the *DS* frame, the position error vector *e* in the *ROV* frame, used as feedback for the vehicle position control loop, is calculated as:

$$\begin{aligned} p_{\text{DP}}^{\text{CAM}} &= p_{\text{DP}}^{\text{DS}} R_{\text{CAM}}^{\text{DS}} + t_{\text{CAM}}^{\text{DS}}, \\ e &= p_{\text{DP}}^{\text{CAM}} R_{\text{ROV}}^{\text{CAM}} + t_{\text{ROV}}^{\text{CAM}}, \end{aligned} \quad (4)$$

where $e = [x_e, y_e, z_e]$.

4.3. ROV control system

Setpoints for ROV surge, sway, depth, and heading control are fed into OceanRINGS⁺ low-level controllers (LLC). OceanRINGS⁺ is a suite of smart technologies for ROV control and subsea operations continuously being developed in house at the Centre for Robotics and Intelligent Systems (CRIS).

OceanRINGS⁺ consists of speed, depth, and heading controllers for subsea navigation and dynamic positioning, and various pilot interfaces with visualisation and situation awareness (Omerdic and Toal, 2012; Toal et al., 2012). The system is designed as a 3-layer ROV control system (Omerdic et al., 2013). Low-level controllers with fault-tolerant control allocation algorithms are part of the bottom layer (Capocci et al., 2018), an interface between an ROV and other supporting platforms is part of the middle layer (e.g. supporting vessels, TMS, image acquisition PC), while supervision, monitoring, and mission planning

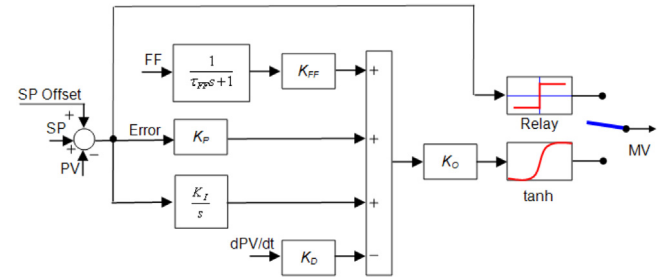


Fig. 11. Internal structure of a LLC loop.

tools are part of the top layer. Based on the camera pose estimation, control parameters are sent to the ROV low-level controllers. Six LLCs control the ROV, each for one degree of freedom (DOF). Surge and Sway controllers are velocity controllers while Heave, Roll, Pitch, and Yaw are position controllers. The internal structure of an LLC loop is shown in Fig. 11.

Modified PID controllers with normalised outputs were used to control the ROV. The difference between setpoints *SPs*, acquired from the image acquisition PC, and process variables *PVs* are used to generate a manipulated variable *MV*. The manipulated variable is applied to drive actuators. If a controller is disabled, the corresponding *MV* is set to zero. In the case of a time-varying *SP*, feed-forward *FF* input is used to improve tracking performance. To avoid problems related to integrator saturation vector *SP_{Offset}* is used. Individual controller outputs are bundled into a vector of normalised forces and moments τ_{LLC} . Since the instruments and equipment onboard are likely to be removed, added or replaced during the trials, the dynamic properties of the ROV change. Therefore for the optimal controller performance, autotuning of the low-level controllers is necessary. The relay output is used for the LLC autotuning with two developed autotuning algorithms. The recorded force-speed static characteristic is utilised for the velocity controllers tuning, while position controllers use self-oscillations approach. The autotuning algorithms and process are explained in more detail in Omerdic et al. (2013).

4.4. Additional considerations

4.4.1. Light marker coverage

In the instance of full or partial occlusion of one or more light beacons, pose estimation is not viable. Such a situation is shown in Fig. 12 with the light beacons fully covered by the ROV tether and the TMS frame. Such a situation can also occur due to other factors, such as fish or curious mammals (e.g. seals, dolphins).

During the docking procedure, the ROV trajectory is always towards the entrance of the TMS, thus it always moves towards the area with better optical marker visibility. As shown in Fig. 13 the algorithms have



Fig. 12. The light markers fully covered (a) by the TMS frame; (b) by the tether.

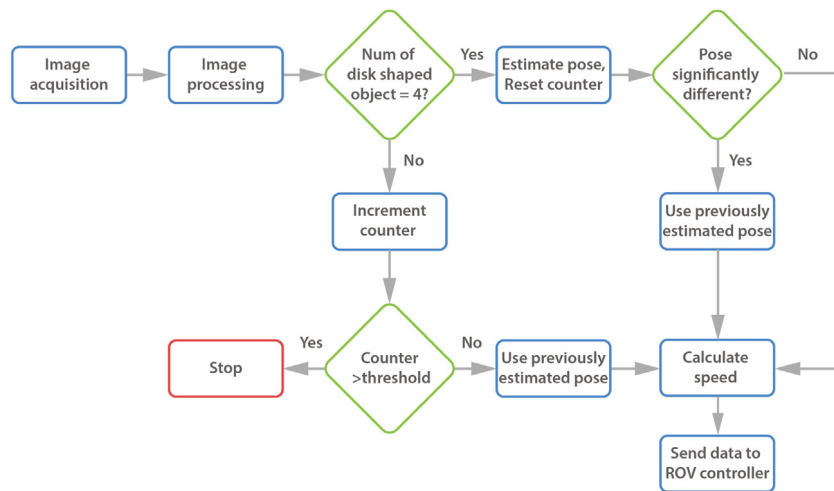


Fig. 13. Flowchart of safety checks.

been implemented to filter pose estimation errors and to protect the system in case such errors become too large.

In case of full coverage of one of the light beacons Fig. 12, the pose cannot be estimated, thus the last known pose is used to align and guide the ROV towards the entrance of the DS. Therefore, by increasing the proximity to the DS, the probability to acquire an image with all markers rises in the next iteration. If the pose cannot be estimated after multiple iterations, the ROV docking manoeuvre is aborted. Due to the slow dynamics of the ROV and low speeds (<0.4 knots) the motion between two consecutive iteration is small, making the described algorithm suitable for this application.

Partial light beacon coverage causes significant pose error, thus every calculated position in step n is compared with the position calculated in step $n-1$. If an unrealistic change in position between two iterations is detected, the algorithm assumes inadequate pose estimation, in which case the last known position is used. An additional light search algorithm is considered to be implemented for future operations.

4.4.2. Low angle measurement sensitivity

Although the discussed pose estimation method provides information on the DS relative orientation and position, initial tests showed low sensitivity to angle measurements. As shown in Fig. 14, the relative heading α_{DS} between the DS and the ROV, maps in the camera projection plane as a perspective distortion of the light marker. For relatively small angles $\alpha_{DS} < 10^\circ$ the perspective distortion in the camera plane is minimal and it is not sufficiently detected due to the camera resolution. The error in the estimation of the angle α_{DS} reflects as ROV pose estimation error. Within close range to the docking station these errors can be neglected. Due to the angle estimation errors the ROV depth

and heading control based on visual pose estimation can cause docking failures. In order to improve autonomous docking performance, the data from the DS heading and depth sensors was used to avoid ROV heading and depth control.

4.4.3. The TMS deployment process for static docking

To test docking to a static target, the TMS was deployed to the seabed. Although static docking is less complicated in terms of control of the vehicle, the risk of damaging equipment was significantly higher since the TMS and the LARS used for the experiment are not designed for such operation. Deployment of assets is a complicated procedure and many factors should be taken into account. Waves, sea currents, and tides act upon the TMS during the deployment process. The TMS used during the trials was not designed for deployment to the seabed thus additional precaution had to be taken.

The deployment of the TMS to the seabed was a challenging task because of the numerous problems that can occur and cause severe damage to the system. The main challenges were:

- Heaving and rolling motion of the ship, transferred through the LARS can cause a heavy impact between the TMS and the seabed in the last few metres before touchdown, thus causing damage
- The umbilical connecting the LARS and the TMS should not be loose because its armour can unwind
- The horizontal movement of the ship must be minimised in order to avoid flipping and damaging the TMS
- Operating from a station-keeping vessel introduces the risk of umbilical and ship thruster entanglement

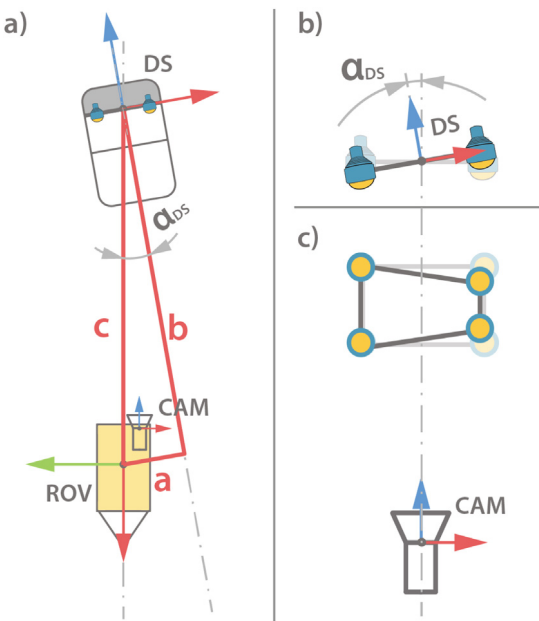


Fig. 14. Relative heading α_{DS} between the DS and the ROV (a) and (b) is measured based on perspective distortion of light beacons in the camera projection plane (c).

When deploying assets to the seabed in high sea states different techniques can be used to compensate for heave motion. There are 'Active' and 'Passive' heave compensation systems (Christ and Sr, 2013). In Active systems, the amount of heave is measured with motion sensors. Depending on the measurement the winch pays out or takes in the umbilical. In passive systems, the umbilical tension is held constant.

Since the LARS used in this case did not have automatic heave compensation, the TMS was deployed during a window of relatively good weather conditions. A few metres of umbilical slack was allowed to compensate for the heaving motion of the ship once the TMS was on the seabed. Attention had to be paid not to release too much umbilical in order to avoid entanglement with the TMS and interference with the ROV operation. The slack also had to be continuously trimmed over time for tidal change.

The umbilical connecting the LARS and the TMS is armoured, and it is designed for a constant tension load (suspended TMS). If a long part of the umbilical gets loose, there is a possibility of armour unwinding which could cause severe damage to the LARS, TMS, and the ROV. Therefore static docking operations were limited to shallow waters.

With a few metres of slack and a relatively short distance between the ship and the TMS, horizontal movement of the ship should not exceed a few metres to avoid flipping the TMS over or dragging it on the seabed. To compensate for that the ship was using its station-keeping system in the highest precision mode. While using station-keeping the ship's thrusters are active, thus additional caution should be taken to avoid contact between loose umbilical and the thrusters. The motion of the ship was within the radius of five metres which allowed us to successfully perform the static docking experiment.

To deploy the TMS on the seabed, the TMS with the ROV inside it was lowered down to 20 m of depth. Altitude was approximately 10 m. The pilot then flew the ROV out of the TMS, which was slowly lowered down while a continuous general visual inspection of the umbilical, seabed, and the TMS was being carried out. Once the TMS was safe on the seabed, experiment was ready to proceed.

5. Results

This section presents the results of offshore docking experiments. Video material of the trials is available on the CRIS YouTube channel (CRIS UL, 2019). Results indicated that visual pose estimation based



Fig. 15. The USBL transponder mounted on the front of the ROV.

autonomous docking of a work class ROV and TMS, in a real-world environment is possible. Both static and dynamic docking experiments were performed during the trials. Although initial camera pose estimation tests were performed earlier (Trslic et al., 2018), the camera pose estimation for ROV control and autonomous docking has never been tested before, thus it was necessary to determine the system performance first.

To validate the performance of the system, the ROV position was measured simultaneously using two different techniques. Camera pose estimation was used for the ROV control as described in Section 4.3. The USBL underwater acoustic positioning system was used for qualitative comparison and monitoring. Such a system consists of an inertial navigational system (INS), coupled with a Doppler Velocity Log (DVL) and USBL transponder, all mounted on the ROV, and a USBL transceiver mounted on the ship. The ROV position measured with the USBL + INS is considered as ground truth, with a measured standard deviation between 0.2 and 0.3 m at all times during the experiment.

In this section, the results of both static and dynamic docking are shown and the ROV approaching procedure for dynamic docking is explained.

5.1. Static docking

To be able to measure the performance of camera estimated relative distance between the ROV and the docking station with the USBL, the position of both must be known. The DS position was recorded prior to the static docking experiment, since only one USBL beacon, attached to the vehicle for continuous monitoring, was provided during the trials, as shown in Fig. 15. It is assumed that the DS position did not change over time.

The experiment started with the ROV placed 4–5 m in front of the DS entrance. The start position was randomly chosen while the light beacons were kept in the camera's FOV. The maximum ROV speed during the experiment was limited to 0.4 knots. The docking station was placed on a rocky seabed at a water depth of approximately 25 m.

Fig. 16 shows the distance x_d and z_d , and the relative heading α_{DS} , between the origin of the ROV frame and the docking point DP during the docking experiment. The orientation of coordinate frames is shown in Fig. 9. Fig. 16(a) shows the distance between the ROV and docking point in XZ-plane. The red line with triangles represents the camera pose estimation while the blue line with circles represents the pose

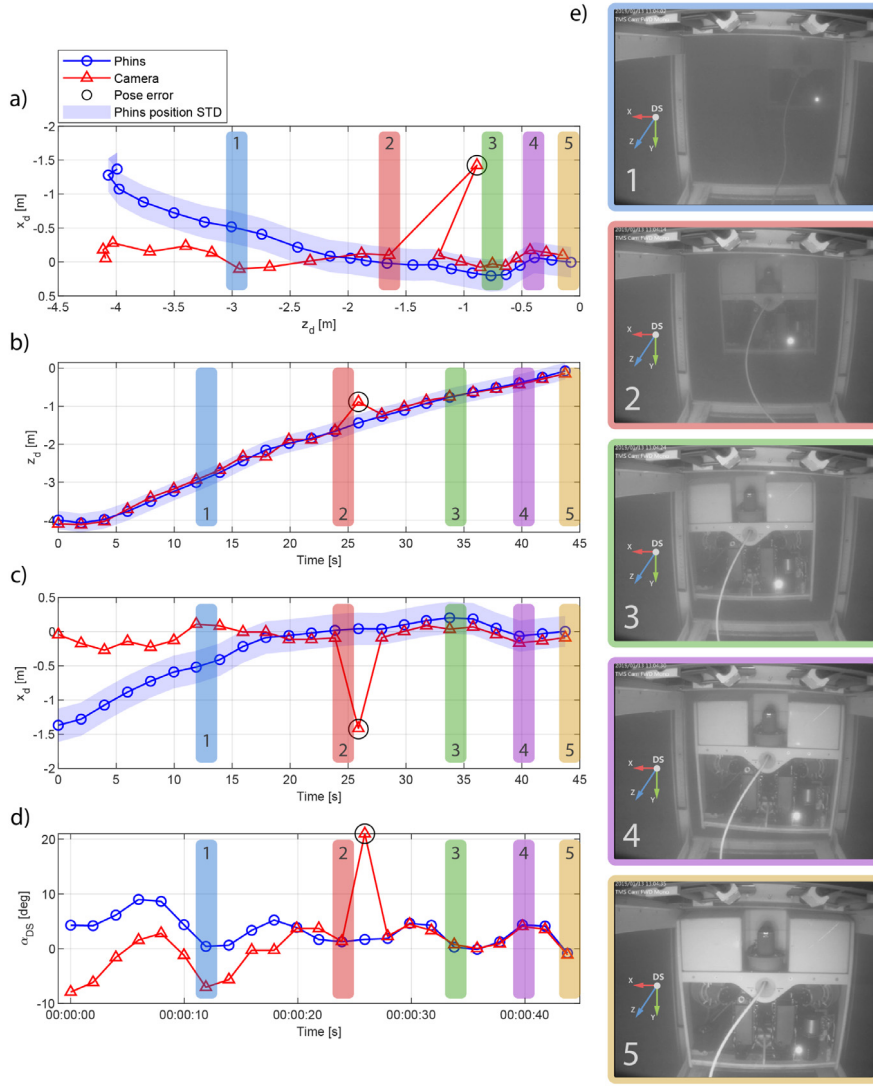


Fig. 16. The distance x_d and z_d between the ROV position and the docking point in the DS frame during static docking. (a) The distance in the XZ-plane; (b) The ROV distance z_d in the DS frame; (c) The ROV distance x_d in the DS frame; (d) Relative heading α_{DS} between the ROV and the DS; (e) A series of images during autonomous docking.

measured with USBL and INS systems. The position standard deviation of the USBL + INS system is showed by blue shaded area. Throughout the experiment the deviation was between 0.22 and 0.25 m. A disparity between the estimated and the true position is present at greater distances, but as the ROV gets closer to the DS, the estimated and true position converge. The disparity is due to the low angle measurement sensitivity, as explained in Section 4.4.2, which is reflected as pose estimation error, particularly in the x_d axis. The distance z_d and x_d plotted against time are shown in (b) and (c). Estimation of z_d shows good performance during the experiment with the estimated position within 0.2 m from the ground truth position at all times. Due to the partial light beacon coverage discussed in Section 4.4, pose estimation errors were present and are shown as spikes in the graphs. In case of a not feasible estimated pose or velocity in step n , the measurement is neglected, and the pose estimated in step $n-1$ is used for ROV control as explained in Fig. 13. Estimated and true relative heading α_{DS} between the ROV and the DS, is shown in (d).

Images (e)_{1–3} show the ROV approaching the DS entrance. The images were acquired with the camera mounted on the DS, at different times during the experiment. The ROV heading is aligned with the DS heading during the approach. The relative heading α_{DS} should be ± 5 deg before the ROV enters the DS (e)₄ in order to dock successfully. Once the ROV stern entered the DS entirely (e)₅, there is only one DOF

between the ROV and the DS left. Since the narrow camera FOV does not allow for pose estimation from a closer distance, and moving the ROV along the z -axis in this position is trivial, the docking experiment is considered successful.

Multiple successful dockings were performed during the trials. Fig. 17 shows the ROV distance from the DP in the XZ-plane during five different dockings. Each docking experiment started from a different position and with a different orientation. The red rectangle shows a region within ± 0.2 m from the centre of the DP frame. When the centre of the ROV coordinate frame is within the region the dock is considered successful.

As mentioned previously, low angle measurement sensitivity at bigger distances from the light marker reflects as a position error, particularly in the x_d axis. Fig. 18(a) shows visual pose estimation error distribution of x_d depending on the relative heading α_{DS} and distance from the docking station z_d . While position error is minimal at the closer distances up to 3 m (light green dots), and it does not depend on the relative heading, at longer distances z_d error grows significantly. Fig. 18(b) shows folded normal distribution of position error $|x_{derr}|$ for range of z_d between 0 and 1.5 m with corresponding mean and standard deviation value. The position error for the range between 1.5 and 3 m is shown in (b) while the distribution of position error in the range between 3 and 4.5 m is shown in (c).

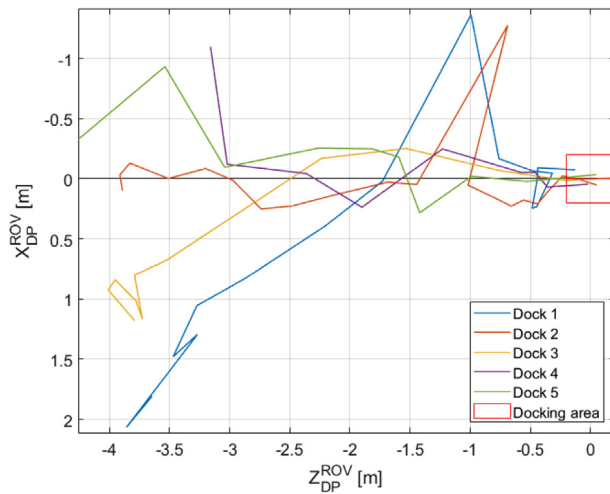


Fig. 17. The estimated ROV position in the DP frame during multiple static dockings.

5.2. Dynamic docking

The ROV position and relative heading in the DP frame during a dynamic docking experiment are shown in Fig. 19. The operating depth was approximately 20 m throughout the experiment. Since one USBL beacon was provided, the comparison between camera pose estimation and USBL position was not viable because of the inability to measure the DS position continuously.

The docking procedure started approximately 2.5 m from the DS entrance (e_1). Partial light beacon coverage caused an error which was detected and the vehicle continued moving towards the DS entrance. The contact between the vehicle and the DS was established (e_2). The ROV position was aligned with the docking station (e_3), and the ROV was docked successfully (e_4). During the experiment the DS was suspended and exposed to the disturbances previously shown in Fig. 1,

thus the docking approach was changed compared to the static docking. Due to inertia, larger mass vehicles react slowly to thruster output, thus it was not feasible to compensate fully for the DS heave motion. Therefore, while static docking was performed with minimal contact between the vehicle and the DS, during dynamic docking the contact is inevitable. Fig. 20 shows the DS heave motion during the experiment.

The peak-to-peak amplitude was approximately 1.1 m with a period of 8.5 s. To dock the vehicle successfully, an average DS depth was calculated and used as the setpoint for ROV depth. There is a limit using this approach. For the DS system used during the trials, the maximum peak to peak amplitude must be lower than the DS entrance height to avoid tether damage. ROVs are designed for harsh environments and able to handle mechanical stress, but it is crucial not to damage the tether.

Fig. 21 shows a series of images during the docking manoeuvre. The ROV in initial docking position starts with the docking manoeuvre (1) and approaches the DS (2)(3). The DS heading has the tendency to change if an external force acts upon it (e.g. contact between the ROV and the DS). After the contact (4) it is important to maintain reverse thrust on the vehicle. The reverse thrust creates momentum around the DS yaw axis and helps with the ROV heading alignment (5)(6)(7). The ROV position is thus aligned in (8)(9). While the vehicle was still reversing back completely aligned, the DS depth changed due to the heave motion and the ROV docked in (10)(11)(12).

The presented docking manoeuvre is the worst case docking scenario since the DS used in these experiments is underactuated (the DS position and orientation are not controllable). While DS pitch and roll are stable, the DS has a tendency to yaw. Since the DS is equipped with an onboard magnetic compass, by adding two thrusters it would be possible to control the DS yaw motion and hence its heading. If the DS heading is controlled and an active heave compensation LARS system is used to compensate for heave motion, the dynamic docking practically reverts to a static docking problem.

6. Conclusion and discussion

Subsea navigation being used in residential ROVs is manual control from the support vessel or from shore-based control centres. With

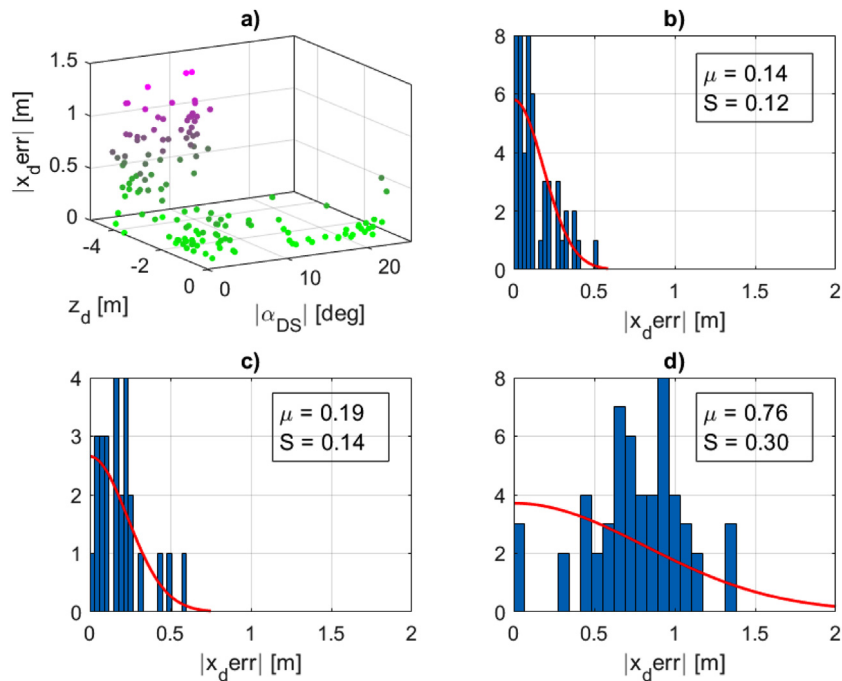


Fig. 18. Folded normal distribution of the position error x_d err during multiple static dockings. (a) Influence of distance and relative heading between ROV and docking point on pose estimation error of x_d ; (b) Distribution of error at distance 0 to 1.5 m from the docking point; (c) Distribution of error at distance 1.5 to 3 m from the docking point; (d) Distribution of error at distance 3 to 4.5 m from the docking point.

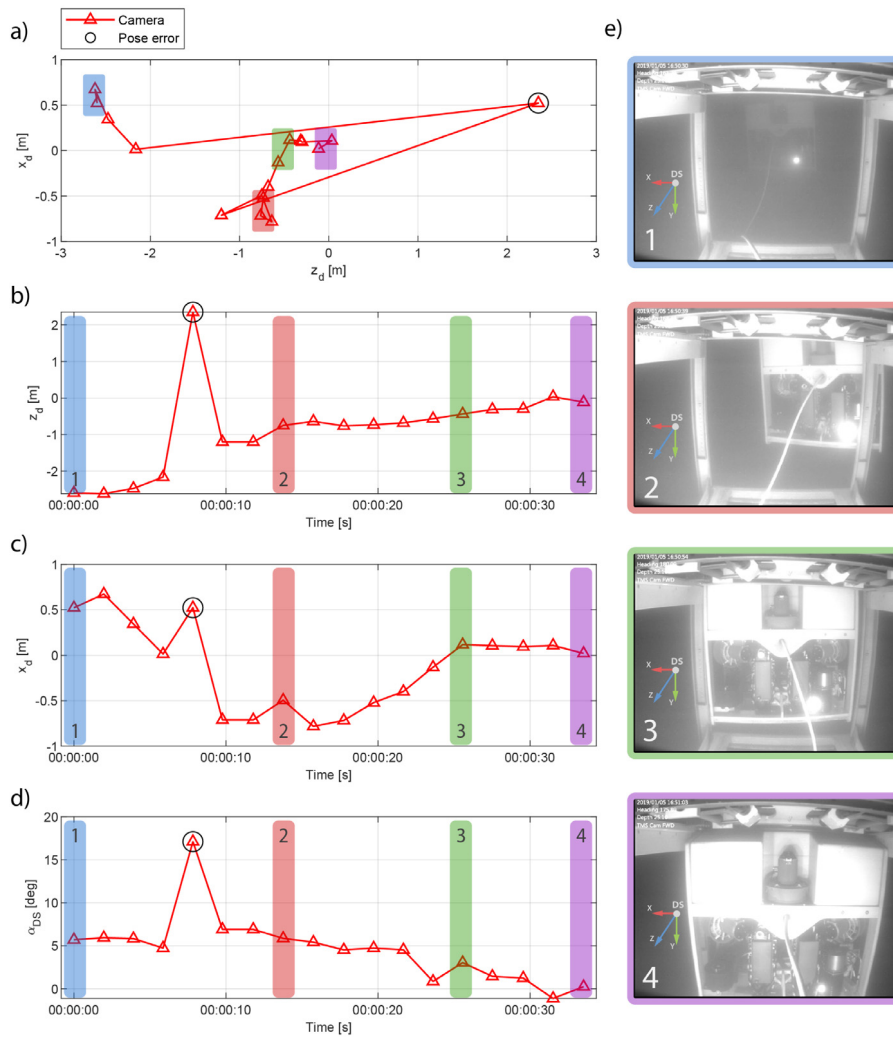


Fig. 19. The distance x_d and z_d between the ROV position and the docking point in the DS frame during dynamic docking. (a) The distance in the XZ -plane; (b) The ROV distance z_d in the DS frame; (c) The ROV distance x_d in the DS frame; (d) Relative heading α_{DS} between ROV and the DS; (e) A series of images during autonomous docking.

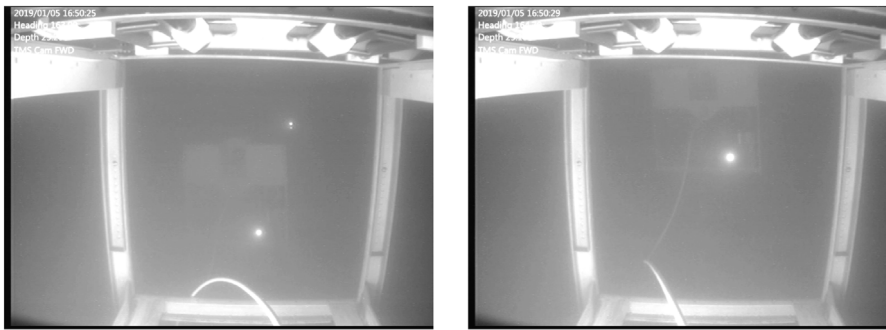


Fig. 20. The DS heaving while the ROV holds constant depth.

an existing fleet of vehicles and experienced ROV pilots as an in-field proven solution, the offshore industry is still hugely dependent on manual pilot skill. However, a transition towards automation in the resident ROV field can provide significant advantages and can specifically increase operational weather windows for the marine IMR sectors. To close this gap, while acknowledging the traditional risk adverse nature of the sector, and to accelerate uptake in resident ROV technology, the existing industry hardware fleet with software upgrades should be utilised. The autonomy needed for a resident ROV should be achieved incrementally through automating specific tasks, while the

ROV pilot role transitions towards supervisory as more and more tasks are automated.

One of the most critical operations is the docking of the ROV at the end of a mission, which was the targeted operation for automation in this paper and research. A machine vision based docking system was developed around subsea camera pose estimation. The system has been developed for standard work-class ROV systems found throughout the sector, deployed from suspended cage type TMS. The relative position between the ROV and the docking station (DS) was estimated using a single camera and a known light marker pattern. The ROV speed and

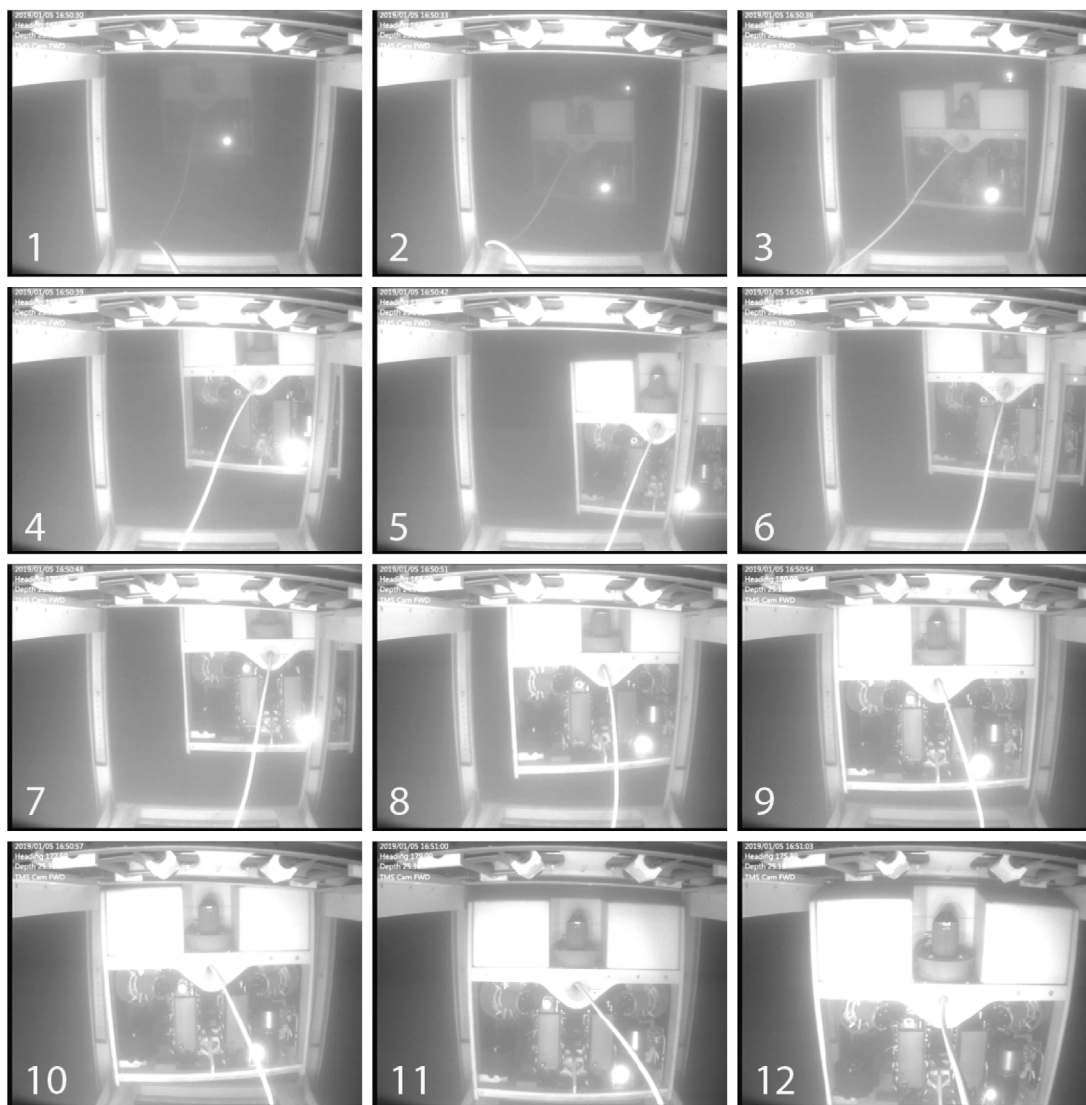


Fig. 21. Dynamic docking to suspended DS.

position controllers, coupled with camera pose estimation, provided a strong platform for such operations. A multi-step pipeline of image acquisition, distortion removal, exposure estimation, Gaussian filter blur and image thresholding allows for the centres of each light beacon within the light marker to be estimated with a high level of precision. The centre points and distances between each beacon then allow for pose estimation of the ROV to the docking station. The position error between docking point DP and origin of the ROV frame is used to calculate setpoints for position and speed controllers which are fed into ROV low-level controllers (LLC). When the DP overlaps with the origin of the ROV frame, the vehicle is considered docked.

The system has been tested and demonstrated in a real-world environment during January 2019 in the North Atlantic Ocean. The reference system used for comparison is commercial state of the art underwater navigation system based on the IXBLUE PHINS INS coupled with Nortek 500 DVL and Teledyne Ranger 2 USBL, and results have shown to be comparable. The accuracy of the developed pose sensor has been shown to be a function of distance from the docking station. It has been shown to be capable of accurately measuring the pose distances and angle up to distances of 4 m. In close proximity, within 1 metre, the differences with the INS solution IXBLUE unit were minimal. The full system including the ROV automated navigational control was trialled first using a static docking station and the results were within tolerances

to allow multiple successful dockings. This system was further tested using a dynamic docking station suspended from surface vessel and the results achieved were sufficient to dock multiple times in heave disturbances due to wave motion of 1.1 m. To dock the vehicle successfully, the maximum peak-to-peak amplitude was found must be lower than 2 m to avoid damaging the ROV tether. To the author's knowledge, this is the first autonomous docking of an ROV system to a dynamic docking station and represents a significant contribution towards robustness and viability of resident ROVs operated using satellite communication channels and overcoming issues such as latency.

The paper presents a visual pose estimation for autonomous docking when in close range, up to 8 m from a docking station. While visual pose estimation performed well during the trials in a low to medium water turbidity, with higher water turbidity, an operation range of the optical sensing becomes limited. In highly turbid water, where a visual pose estimation is unavailable, the acoustic pose estimation based on USBL/LBL technology should be used. Since the precision of acoustic-based positioning systems is lower than vision-based systems, the docking station entrance should be modified. The extended, funnel-shaped entrance allows for a larger position error and helps to physically guide the vehicle.

Future developments within the automated docking system are focused on the quality of camera pose estimation and suspended TMS

motion replication, relying on the work of Rossi et al. (2018), Palomeras et al. (2018), Sivčev et al. (2018). The method based on a stereo camera pair using the StereoFusion algorithm for real-time 3D dense reconstruction and camera tracking will improve position estimation quality and overcome the marker detection problem due to the light beacon occlusion. Fusing data from the onboard inertial navigation system with vision-based navigation will contribute to system robustness and accuracy while a TMS motion replication could partially compensate for suspended TMS heave motion, allowing for faster and smoother docking. Additional thrusters could be attached to the TMS for better yaw motion stability, while a wide-angle camera lens and a dome port on the camera housing should be used to expand the camera's FOV.

Declaration of competing interest

The authors declare that they have no known competing financial interests or personal relationships that could have appeared to influence the work reported in this paper.

Acknowledgements

This material is based upon works supported by Science Foundation Ireland and industry partners Shannon Foynes Port Company and The Commissioners of Irish Lights, Ireland under the MaREI Research Centres Awards 12/RC/2302_P2 & 14/SP/2740, RoboVaaS EU ERA-Net Co-fund award through Irish Marine Institute and EU Horizon 2020 research and innovation programme project EUMarineRobots under grant agreement 731103.

References

- Allen, B., Austin, T., Forrester, N., Goldsborough, R., Kukulya, A., Packard, G., Purcell, M., Stokey, R., 2006. Autonomous docking demonstrations with enhanced REMUS technology. In: OCEANS 2006, pp. 1–6. <http://dx.doi.org/10.1109/OCEANS.2006.306952>.
- Bosch, J., Gracias, N., Ridao, P., Istenič, K., Ribas, D., 2016. Close-range tracking of underwater vehicles using light beacons. Sensors 16 (4), 429. <http://dx.doi.org/10.3390/s16040429>, URL <https://www.mdpi.com/1424-8220/16/4/429>.
- Buffagni, M., Gasparoni, F., Bergseth, N.H., Bjornbom, E., Broccia, P., 2014. Development and Test of an AUV for Environmental Monitoring and Asset Integrity in Offshore O&G Scenarios: CLEAN SEA Project. Society of Petroleum Engineers, <http://dx.doi.org/10.2118/168471-MS>.
- Caiti, A., Ciaramella, E., Conte, G., Cossu, G., Costa, D., Grechi, S., Nuti, R., Scaradozzi, D., Sturniolo, A., 2016. OptoCOMM: introducing a new optical underwater wireless communication modem. In: 2016 IEEE Third Underwater Communications and Networking Conference (UComms). IEEE, pp. 1–5.
- Capocci, R., Omerdic, E., Dooly, G., Toal, D., 2018. Fault-tolerant control for ROVs using control reallocation and power isolation. J. Mar. Sci. Eng. 6 (2), 40. <http://dx.doi.org/10.3390/jmse020040>, URL <https://www.mdpi.com/2077-1312/6/2/40>.
- Chan, R.H., Ho, C.-W., Nikolova, M., 2005. Salt-and-pepper noise removal by median-type noise detectors and detail-preserving regularization. IEEE Trans. Image Process. 14 (10), 1479–1485.
- Christ, R.D., Sr, R.L.W., 2013. The ROV Manual: A User Guide for Remotely Operated Vehicles. Butterworth-Heinemann.
- Conte, G., Scaradozzi, D., Mannochi, D., Raspa, P., Panebianco, L., et al., 2016. Development and testing of low-cost ASV. In: The 26th International Ocean and Polar Engineering Conference. International Society of Offshore and Polar Engineers.
- Cowen, S., Briest, S., Dombrowski, J., 1997. Underwater docking of autonomous underwater vehicles using optical terminal guidance. In: Oceans '97. MTS/IEEE Conference Proceedings, vol. 2, pp. 1143–1147. <http://dx.doi.org/10.1109/OCEANS.1997.624153>.
- CRIS UL, CRIS UL, 2019. Work class ROV vision based autonomous docking [video file]. URL <https://www.youtube.com/watch?v=ypgwMfDN6U&feature=youtu.be>.
- Dooly, G., Omerdic, E., Coleman, J., Miller, L., Kaknjo, A., Hayes, J., Braga, J., Ferreira, F., Conlon, H., Barry, H., et al., 2016. Unmanned vehicles for maritime spill response case study: Exercise cathach. Mar. Pollution Bull. 110 (1), 528–538.
- Dudley, B., 2018. BP Statistical Review of World Energy. Tech. Rep., British Petroleum, p. 56, URL <https://www.bp.com/content/dam/bp/business-sites/en/global/corporate/pdfs/energy-economics/statistical-review/bp-stats-review-2018-full-report.pdf>.
- Duntley, S.Q., 1963. Light in the sea. JOSA 53 (2), 214–233.
- Equinor, 2019. Equinor E-ROV concept, SV version [video file]. URL <https://www.youtube.com/watch?v=OdLSBTIHkU0>.
- Esakkirajan, S., Veerakumar, T., Subramanyam, A.N., PremChand, C., 2011. Removal of high density salt and pepper noise through modified decision based unsymmetric trimmed median filter. IEEE Signal Process. Lett. 18 (5), 287–290.
- Feezor, M.D., Sorrell, F.Y., Blankinship, P.R., Bellingham, J.G., 2001. Autonomous underwater vehicle homing/docking via electromagnetic guidance. IEEE J. Ocean. Eng. 26 (4), 515–521. <http://dx.doi.org/10.1109/48.972086>.
- Fehse, W., 2003. Automated Rendezvous and Docking of Spacecraft. vol. 16, Cambridge University Press.
- Ferri, G., Djapic, V., 2013. Adaptive mission planning for cooperative autonomous maritime vehicles. In: 2013 IEEE International Conference on Robotics and Automation. IEEE, pp. 5586–5592.
- Fornai, F., Toal, D., Omerdic, E., Dooly, G., Ferri, G., 2013. A novel self-locking mechanism to connect two ROVs. In: 2013 MTS/IEEE OCEANS-Bergen. IEEE, pp. 1–4.
- Gracias, N., Bosch, J., Karim, M.E., 2015. Pose estimation for underwater vehicles using light beacons. In: 4th IFAC Workshop on Navigation, Guidance and Control of Underwater VehiclesNGCUV 2015. IFAC-PapersOnLine 48 (2), 70–75. <http://dx.doi.org/10.1016/j.ifacol.2015.06.012>, URL <http://www.sciencedirect.com/science/article/pii/S2405896315002517>.
- Grasso, T., Bruni, F., Filippini, M., Gasparoni, F., Maddalena, D., Miozza, L., Cioffi, P., Lainati, A., Rimoldi, A., Gentile, L., Di Fede, G., 2016. Clean Sea hybrid ROV/AUV for Asset Integrity Operations. International Society of Offshore and Polar Engineers.
- Haltrin, V.I., 1999. Chlorophyll-based model of seawater optical properties. Appl. Opt. 38 (33), 6826–6832.
- Hartley, R., Zisserman, A., 2004. Multiple View Geometry in Computer Vision. Cambridge University Press, Google-Books-ID: e30hAwAAQBAJ.
- IKM Subsea, 2018. R-ROV and OCC from IKM [video file]. URL https://www.youtube.com/watch?time_continue=12&v=nvHS7aV5A8Q.
- Intelligence, M., M. Intelligence, 2019. ROV Market - Segmented by Type, Activity, Application Industry, and Geography - Growth, Trends and Forecast (2019 - 2024). Tech. Rep., URL <https://www.mordorintelligence.com/industry-reports/rov-market>.
- Krupinski, S., Maurelli, F., Grenon, G., Petillot, Y., 2008. Investigation of autonomous docking strategies for robotic operation on intervention panels. In: OCEANS 2008, pp. 1–10. <http://dx.doi.org/10.1109/OCEANS.2008.5151995>.
- Lee, D., Kim, G., Kim, D., Myung, H., Choi, H.-T., 2012. Vision-based object detection and tracking for autonomous navigation of underwater robots. Ocean Eng. 48, 59–68.
- Li, Y., Jiang, Y., Cao, J., Wang, B., Li, Y., 2015. AUV docking experiments based on vision positioning using two cameras. Ocean Eng. 110, 163–173. <http://dx.doi.org/10.1016/j.oceaneng.2015.10.015>, URL <http://www.sciencedirect.com/science/article/pii/S0029801815005521>.
- Liljebäck, P., Mills, R., 2017. Eelume: A flexible and subsea resident IMR vehicle. In: OCEANS 2017 - Aberdeen, pp. 1–4. <http://dx.doi.org/10.1109/OCEANSE.2017.8084826>.
- Liu, S., Ozay, M., Okatanı, T., Xu, H., Sun, K., Lin, Y., 2018. Detection and pose estimation for short-range vision-based underwater docking. IEEE Access 7, 2720–2749.
- Liu, S., Xu, H., Lin, Y., Gao, L., 2019a. Visual navigation for recovering an AUV by another AUV in shallow water. Sensors 19 (8), 1889.
- Liu, G., Xu, C., Zhu, Y., Zhao, J., 2019b. Monocular vision-based pose determination in close proximity for low impact docking. Sensors 19 (15), 3261.
- Łuczyński, T., Pfingsthorn, M., Birk, A., 2017. The Pinax-model for accurate and efficient refraction correction of underwater cameras in flat-pane housings. Ocean Eng. 133, 9–22. <http://dx.doi.org/10.1016/j.oceaneng.2017.01.029>, URL <http://www.sciencedirect.com/science/article/pii/S0029801817300434>.
2019. Research vessel RV celtic explorer. URL <https://www.marine.ie/Home/site-area-infrastructure-facilities/research-vessels/celtic-explorer>,
- Mokuno, M., Kawano, I., 2011. In-orbit demonstration of an optical navigation system for autonomous rendezvous docking. J. Spacecr. Rockets 48 (6), 1046–1054.
- Oceanengineering, 2019. E-ROV System. URL <https://www.oceanengineering.com/brochures/e-rov-system/>.
- Omerdic, E., Toal, D., 2012. OceanRINGS: System concept applications. In: 2012 20th Mediterranean Conference on Control Automation (MED), pp. 1391–1396. <http://dx.doi.org/10.1109/MED.2012.6265833>.
- Omerdic, E., Toal, D., Dooly, G., 2013. OceanRINGS: Smart technologies for subsea operations. In: Advanced in Marine Robotics. LAP LAMBERT Academic Publishing.
- Omerdic, E., Toal, D., Dooly, G., Kaknjo, A., 2014. Remote presence: Long endurance robotic systems for routine inspection of offshore subsea oil & gas installations and marine renewable energy devices. In: 2014 Oceans-St. John'S. IEEE, pp. 1–9.
- OSJ, 2018. Resident robots could save money and remove ships from the equation. OSJ - Offshore Support J. 21 (4), 26–28, URL https://issuu.com/rivieramaritimemedia/docs/offshore_support_journal_may_2018.
- Palomeras, N., Vallicrosa, G., Mallios, A., Bosch, J., Vidal, E., Hurtos, N., Carreras, M., Ridao, P., 2018. AUV homing and docking for remote operations. Ocean Eng. 154, 106–120. <http://dx.doi.org/10.1016/j.oceaneng.2018.01.114>, URL <http://www.sciencedirect.com/science/article/pii/S0029801818301367>.

- Park, J.-Y., Jun, B.-h., Lee, P.-m., Oh, J., 2009. Experiments on vision guided docking of an autonomous underwater vehicle using one camera. In: Autonomous Underwater Vehicles. *Ocean Eng.* 36 (1), 48–61. <http://dx.doi.org/10.1016/j.oceaneng.2008.10.001>, URL <http://www.sciencedirect.com/science/article/pii/S0029801808002242>.
- Pontbriand, C., Farr, N., Ware, J., Preisig, J., Popenoe, H., 2008. Diffuse high-bandwidth optical communications. In: *OCEANS 2008*. IEEE, pp. 1–4.
- Robinson, L., Newe, T., Burke, J., Dooly, G., Coleman, J., Toal, D., 2018. High bandwidth maritime communication systems – Review of existing solutions and new proposals. In: 2018 2nd URSI Atlantic Radio Science Meeting (AT-RASC), pp. 1–3. <http://dx.doi.org/10.23919/URSI-AT-RASC.2018.8471655>.
- Rossi, M., Trsljic, P., Sivčev, S., Riordan, J., Toal, D., Dooly, G., 2018. Real-time underwater StereoFusion. *Sensors* 18 (11), 3936. <http://dx.doi.org/10.3390/s18113936>, URL <https://www.mdpi.com/1424-8220/18/11/3936>.
- Sivčev, S., Rossi, M., Coleman, J., Dooly, G., Omerdić, E., Toal, D., 2018. Fully automatic visual servoing control for work-class marine intervention ROVs. *Control Eng. Pract.* 74, 153–167.
- Sivčev, S., Omerdić, E., Dooly, G., Coleman, J., Toal, D., 2018. Towards inspection of marine energy devices using ROVs: floating wind turbine motion replication. In: Ollero, A., Sanfeliu, A., Montano, L., Lau, N., Cardeira, C. (Eds.), *ROBOT 2017: Third Iberian Robotics Conference*. In: *Advances in Intelligent Systems and Computing*. Springer International Publishing, pp. 196–211.
- Statoil, 2017. How we think UIDs will be used by statoil in the future. URL https://32zn56499nov99m251h4e9t8-wpengine.netdna-ssl.com/wp-content/uploads/2017/07/ID2017_Att09_Statoil_TomGlancy.pdf.
- Toal, Omerdic, Ahmad, Nolan, 2012. ROV LATIS: next generation smart underwater vehicle. In: Roberts, Sutton (Eds.), *Further Advances in Unmanned Marine Vehicles*. Institution of Engineering and Technology, pp. 9–44. http://dx.doi.org/10.1049/PBCE077E_ch2, URL https://digital-library.theiet.org/content/books/10.1049/pbce077e_ch2.
- Trsljic, P., Rossi, M., Sivčev, S., Dooly, G., Coleman, J., Omerdić, E., Toal, D., 2018. Long term, inspection class ROV deployment approach for remote monitoring and inspection. In: *OCEANS 2018 MTS/IEEE Charleston*. IEEE, Charleston, SC, pp. 1–6. <http://dx.doi.org/10.1109/OCEANS.2018.8604814>, URL <https://ieeexplore.ieee.org/document/8604814/>.
- uEye Camera Interface in Matlab, 2016. URL <http://matlabtidbits.blogspot.com/2016/10/ueye-camera-interface-in-matlab-mex.html>.
- UT2, 2018. UT3 - resident ROVs. UT2 12 (4), 26–31, URL https://issuu.com/ut_2_publication/docs/issuu_2108_4_front_cover.
- Vallicrosa, G., Bosch, J., Palomeras, N., Ridao, P., Carreras, M., Gracias, N., 2016. Autonomous homing and docking for AUVs using range-only localization and light beacons. In: *10th IFAC Conference on Control Applications in Marine SystemsCAMS 2016*. IFAC-PapersOnLine 49 (23), 54–60. <http://dx.doi.org/10.1016/j.ifacol.2016.10.321>, URL <http://www.sciencedirect.com/science/article/pii/S2405896316319085>.
- W. Europe, 2017. Floating Offshore Wind Vision Statement. Tech. Rep., Wind Europe, URL <https://windeurope.org/wp-content/uploads/files/about-wind/reports/Floating-offshore-statement.pdf>.
- Yu, F., He, Z., Qiao, B., Yu, X., 2014. Stereo-vision-based relative pose estimation for the rendezvous and docking of noncooperative satellites. *Math. Probl. Eng.* 2014.
- Zhong, L., Li, D., Lin, M., Lin, R., Yang, C., 2019. A fast binocular localisation method for AUV docking. *Sensors* 19 (7), 1735.